IEEE Access
Multidisciplinary ⋮ Rapid Review ⋮ Open Access Journal

Received September 16, 2019, accepted October 3, 2019, date of publication October 30, 2019,
date of current version December 23, 2019.

Digital Object Identifier 10.1109/ACCESS.2019.2950391

Research on Prediction of Metro Wheel Wear Based on Integrated Data-Model-Driven Approach

AIHUA ZHU[1,2], SI YANG[2], QIANG LI[1], JIANWEI YANG[2], CAOZHENG FU[2], JIAO ZHANG[3], AND DECHEN YAO[2]

[1]School of Mechanical and Electronic Control Engineering, Beijing Jiaotong University, Beijing 100044, China
[2]Beijing Key Laboratory of Performance Guarantee on Urban Rail Transit Vehicles, Beijing University of Civil Engineering and Architecture, Beijing 100044, China
[3]Beijing subway Operation Technology Centre, Beijing 102208, China

Corresponding author: Qiang Li (qli3@bjtu.edu.cn)

This work was supported in part by the National Natural Science Foundation of China under Grant 51605023 and Grant 51975038, in part by the Talent Projects in Organization Department, Beijing Municipal Party Committee under Grant 2012D005017000006, and in part by the Fundamental Research Funds for Beijing University of Civil Engineering and Architecture under Grant X18207.

ABSTRACT Existing research on wheel wear prediction uses either data-driven or model-based methods. However, due to the high reliability and limited sample characteristics of metro wheel wear, data-driven methods are not accurate enough and require relatively high data costs, and model-based methods mainly lack verification with measured data and generalization ability. To address the shortcomings of the two types of methods, a new approach combining model-based and data-driven methods is used to predict wheel wear in this paper. First, the least-squares algorithm is used to analyze and calculate the difference between the wear measurement for a specific running mileage and the corresponding simulated wear, with the minimum difference taken as an objective function. By means of optimization algorithms including Genetic Algorithm, Particle Swarm Optimization, Tabu Search and Simulated Annealing, the wear coefficient k in Jendel wear model is optimized, thereby obtaining an optimized Jendel wear model. Later, metro wheel wear for additional running mileage is simulated and predicted through combined application of the vehicle system dynamics, wheel-rail contact, and optimized Jendel wear models. Finally, the paper analyzes the wear prediction results obtained by the integrated data-model-driven approach and compares them with the results of traditional methods and measured data. The results suggest that the integrated data-model-driven approach effectively reduces the uncertainty in selecting the wear coefficient by experience, lowers the experimental data costs, and improves the wear prediction accuracy. Therefore, it is a promising approach to wheel wear prediction.

INDEX TERMS Metro wheel, wear prediction, data-model driven, optimization algorithms, Jendel wear model.

I. INTRODUCTION

Prognostics and health management (PHM) technology can be adopted to predict the state of a system with sound functions and make reasonable decisions concerning maintenance based on the predicted information [1]. It is one of the core technologies applied in reliability and systems engineering, which covers numerous fields and disciplines, including mechanical materials, automation, reliability, and artificial intelligence. Existing prediction schemes are classified into two categories: schemes based on physical models and data-driven schemes [2], [3].

In model-based prediction methods, the state of the system is predicted using models developed with physical equipment, such as the spatial response and failure mechanism models [4]. Such methods are not dependent on large amounts of equipment's health data for different stages. In order to ensure precision of system predictions, it is necessary to determine the parameters for physical models that characterize the system's faults in a better manner. However, it is often

The associate editor coordinating the review of this manuscript and approving it for publication was Nagarajan Raghavan.

difficult to take into consideration all actual operational conditions of equipment and to comprehensively and precisely obtain the parameters involved in the physical models [5], [6].

A data-driven prediction method consists of an artificial intelligence algorithm and probability statistics. This prediction method can provide a timely representation of changes in equipment performance based on efficient use of equipment or systematic sound information contained in the test and monitored data from different stages (including system design, simulation, operation, and maintenance), so as to obtain residual life function of the system and help decision-making [7]. In 2013, Tamilselvan and Wang [8] presented a novel multi-sensor health diagnosis approach using deep belief network (DBN) based state classification. In 2016, Li *et al.* [9] used a deep random forest fusion (DRFF) method to improve the performance of gearbox fault diagnosis using both acoustic and vibratory signals. In 2018, Peimankar *et al.* [10] presented an ensemble time series forecasting algorithm which uses evolutionary multi-objective optimization algorithms to predict dissolved gas contents in power transformers. These data-driven methods do not require an in-depth understanding of the internal operating and failure mechanisms of an equipment system. However, for equipment that provides high reliability, small samples, and deficient information, this method is not accurate enough and the data costs are relatively high [11], [12].

In recent years, scholars have proposed a new failure prediction technology that complements and integrates the two approaches to address their shortcomings [13]. The integration of the physical model and data-driven methods significantly increases the prediction efficiency and precision and reduces the cost [14], [15].

Wheel wear is a typical form of failure of railway wheel rail system. Some research has been conducted on service life prediction for railway vehicle wheels using a data-driven method. In one study [16], [17], a Monte Carlo statistical method was adopted to predict the service life of wheels from significant amounts of measured wheel wear data from the Guangzhou Metro. In 2015, based on the data obtained from a knowledge base and the fuzzy logic system, Dordević *et al.* [18] analyzed the influence of various factors on rolling stock failure, and evaluated the reliability of wheels. Andrade and Stow [19] applied linear statistics to analyze and predict railway wheel data, and determined the optimal wheel parameter values required for rolling 250,000 km without turning repair. On this basis, Han and Zhang [20] predicted the wheel wear of the track by polynomial fitting.

There is also a great deal of research that looks at wheel wear prediction using the model-based methods. In 2013, Ding *et al.* [21] and Tao *et al.* [22] predicted the residual service life of wheels through a simulation method that uses the SIMPACK vehicle system dynamics software SIMPACK combined with the wheel-rail contact and wheel wear models. With rapidly increasing railway traffic around the world, traditional post-maintenance of railway equipment has been upgraded to preventive maintenance, such as reliability-centered maintenance (RCM) [23]. Owing to the recent global application of RCM technology in railway traffic, there is growing demand for vehicle safety and comfort shortening of the cycle of wheel turning repair. Within this context, scholars from different countries have begun to pay great attention to wheel wear prediction for metro vehicles with short-term service. In 2017, scholars provided improved wear prediction models with less wear calculation time and higher precision of prediction [24], [25].

The research on data-driven wheel wear prediction mentioned above relies on large amounts of wear data measured in the absence of turning repair as well as statistical methods for wheel wear prediction, and thus its cost is bound to be high. As RCM technology is still under development, it is difficult to obtain scientific, high-quality, and accurate wheel wear predictions with data-driven methods.

The wheel wear prediction method based on a physical model mainly lacks verification with measured data, as well as generalization ability. The parametric modeling method makes it difficult to take into account all possible complicated changes that may occur during actual vehicle operation; thus, reasonable data processing is required for optimization and improvement.

To address the shortcomings of the above two methods, this paper combines model-based and data-driven methods to predict metro wheel wear. The integrated data-model-driven approach reduces the data costs and improves the accuracy and generalization abilities of the models.

This paper is organized as follows. Section I introduces the research background and significance of this paper. Section II presents the process of wheel wear prediction based on data-model-driven integration. Section III reviews the Jendel wear model and wear coefficient k. In Section IV, the wear coefficient k in the Jendel wear model is optimized using Genetic Algorithm (GA), Particle Swarm Optimization (PSO), Tabu Search (TS) and Simulated Annealing (SA), separately, with the measured wheel wear data for a specific running mileage being used as the training sample. In Section V, the metro wheel wear for additional running mileage is simulated and predicted through a combined application of the vehicle system dynamics, wheel-rail contact, and optimized Jendel wear models. Section VI analyzes the wear prediction results obtained by the integrated data-model-driven approach and compares them with the results obtained with traditional methods and measured data. Finally, Section VII summarizes the conclusions reached in this paper.

II. PROCESS OF WHEEL WEAR PREDICTION METHOD BASED ON DATA-MODEL-DRIVEN INTEGRATION

A. DATA-DRIVEN OPTIMIZATION OF WEAR MODEL

The actual wear data were obtained from a vehicle with mileage of 50,000 km. Then, the software Matlab was used to compile the Jendel wear model for subsequent simulation calculation of vehicle wheel wear for 50,000 km.

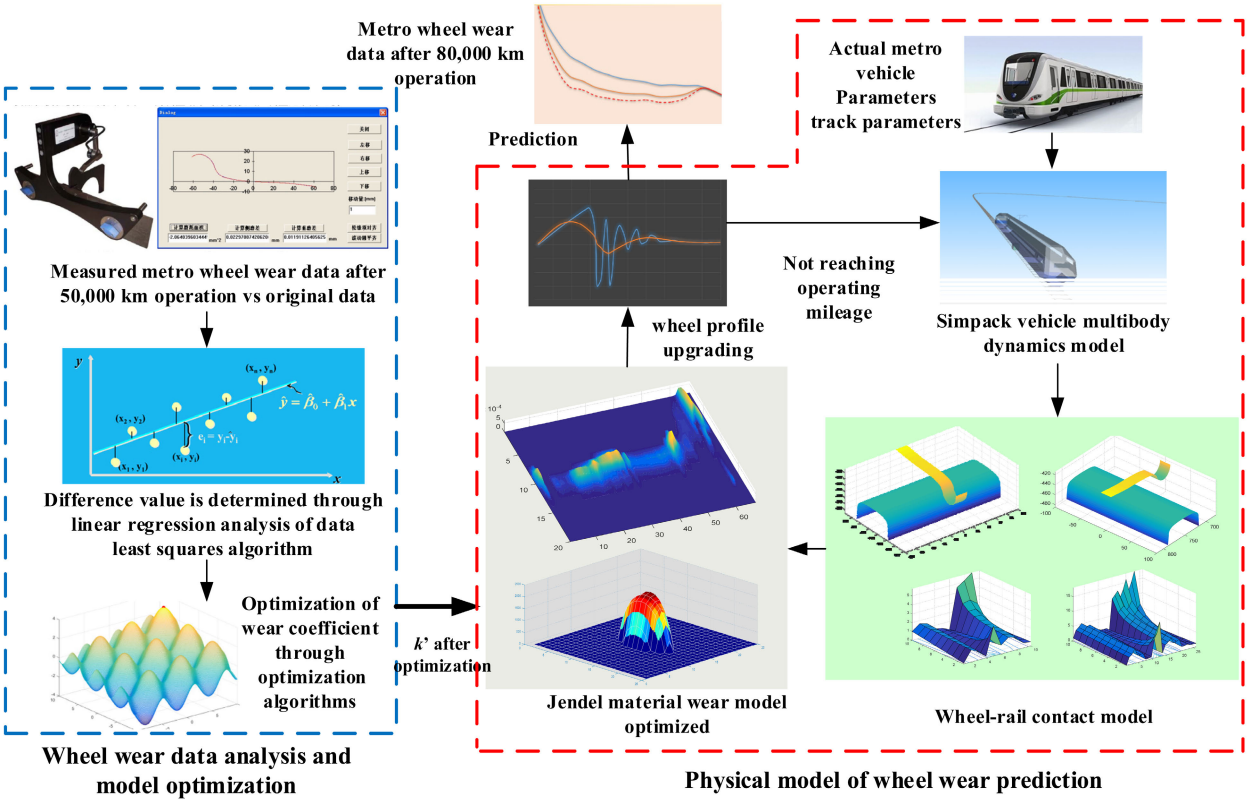

FIGURE 1. Schematic of wheel wear simulation and prediction based on data-model-driven integration.

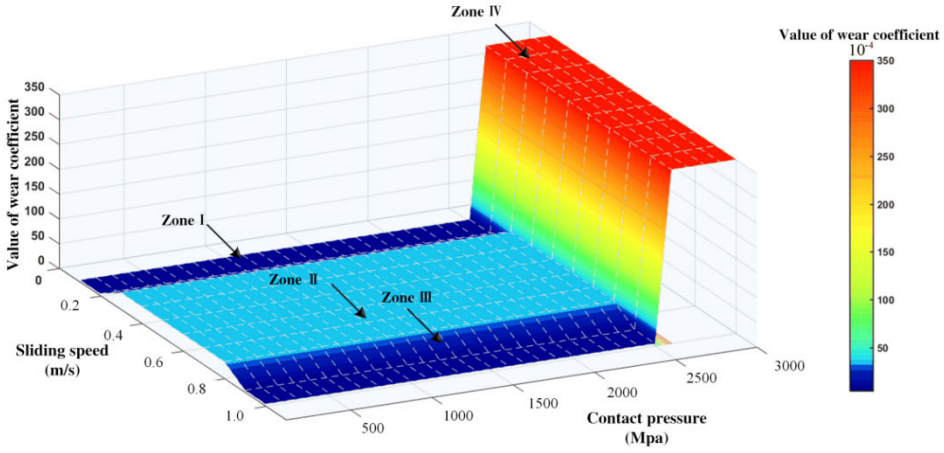

FIGURE 2. Relationship between wear coefficient, and contact stress and sliding speed.

Thereafter, we calculated the difference between the measured and simulated wear values using the theory of regression and the least-squares algorithm, and the least difference was taken as the objective function. The optimal value for the Jendel model's wear coefficient k was determined by means of Genetic Algorithm (GA), Particle Swarm Optimization (PSO), Tabu Search (TS) and Simulated Annealing (SA); accordingly, the optimized Jendel model was obtained. A flow diagram of the process is shown in the left of Figure 1.

B. VEHICLE MODEL CONSTRUCTION AND WEAR SIMULATION CALCULATION

After the data-driven optimization was completed, model-based wear prediction was performed using physical models, including a multi-body dynamics model, wheel-rail contact model, optimized Jendel wear model, and wheel tread upgrading model. This process is illustrated in the right of Figure 2.

First, the actual vehicle and track parameters were input into SIMPACK to construct a vehicle multi-body dynamics

model. The vehicle dynamics model was then used to calculate the spatial geometry of wheel-rail contact.

Later, the wheel-rail contact model was applied for detailed calculation of the wheel-rail contact patch, creep force distribution and other parameters. The normal and tangential forces at wheel-rail contact were obtained.

Next, the results from the wheel-rail contact model were input into the optimized Jendel wear model to calculate wheel wear.

As wheel profile will change after the vehicle travels a certain distance, smoothing was performed on the worn wheel profile. The resulting new wheel profile was then input into the vehicle dynamics model to upgrade the original profile for cyclic wear calculation.

Then wheel wear for other running mileage (e.g. 80,000 km) is simulated and predicted through combined application of the vehicle system dynamics, wheel-rail contact, and optimized Jendel wear models.

III. JENDEL WEAR MODEL

The Archard model [26] is used extensively to analyze the wear caused by rolling and sliding contact. It is considered that the material wear loss V_A is directly proportional to the coefficient of wear k, contact normal pressure N, and relative sliding distance d, while it is inversely proportional to the hardness H of the worn material. It is given by

$$V_{\mathrm{A}} = k\frac{Nd}{H}, \tag{1}$$

In order to determine the wear coefficient uncertainty, a series of experimental data were collected by Jendel on the basis of Archard's theory of wear in rolling contact. Jendel developed the wheel tread wear model in 2002, and determined the wear coefficient values for different types of contact. In the Jendel model [27], the wear coefficient is related to the sliding speed and contact stress, as indicated in Figure 2.

The wear coefficient k is determined from experimental statistics. When the contact pressure and stress limits are below 0.8 H, three zones can be recognized based on sliding speed. In zone I, the sliding speed is relatively low, indicating slight wear, and the wear coefficient k_1 ranges from 1×10^{-4} to 10×10^{-4}. In zone II, the sliding speed varies from 0.2 to 0.7 m/s, indicating serious wear, and the wear coefficient k_2 ranges from 30×10^{-4} to 40×10^{-4}. In zone III, the sliding speed is high and a temperature increase in this zone results in a decline in the wear coefficient k_3, whose range is close to that in the slight wear zone (1×10^{-4} to 10×10^{-4}). The contact pressure and stress in zone IV exceed the limit value of 0.8 H, indicating occurrence of destructive wear.

The wear coefficient k_4 increases significantly, ranging from 300×10^{-4} to 400×10^{-4}.

A majority of scholars have selected the value of wear coefficient k according to their experience. In [22] and [28], a mean value of k was adopted for zones I to III. [29] only considered the condition of k in zone I, which was set at 1.09×10^{-4}. In [30], a higher k value was adopted in the boundary area. There are uncertainties in these k values as they were determined only by experience.

By simulating actual tracks, scholars have obtained experimental wear data, conducted research on the wear coefficient k in the Jendel model using a statistical method, and developed wear coefficient probability graphs applicable to specific track and wheel materials in recent years [31], [32]. These graphs are more detailed compared to the diagram showing the wear coefficient distribution determined by statistics using the Jendel model. The statistical method described above needs to be supported by large amounts of experimental data, significantly increasing the cost of data acquisition. Moreover, the experimentally simulated data cannot accurately reflect the state of wheel running on an actual track. The confidence interval for the wear coefficient is also less instructive for wheels on other tracks.

In this study, 50,000 km wheel wear data measured from an actual track were used as the training sample, and optimization algorithms were applied to optimize the wear coefficient k in the Jendel wear model and reduce its uncertainty.

IV. WHEEL WEAR DATA ANALYSIS AND MODEL OPTIMIZATION

First, the measured wheel wear data for running mileage of 5000 km was analyzed and used as the training sample. Next, the wear coefficient in the Jendel wear model described in Section III was optimized using optimization algorithms.

Genetic Algorithm (GA), Particle Swarm Optimization (PSO), Simulated Annealing (SA) and Tabu Search (TS) were applied, separately. Over decades of development, these algorithms have become well-developed classical intelligent optimization algorithms with good reliability and robustness features. Many researchers have verified and improved their performance and widely applied them to practical problems like combinatorial optimization.

A. ACQUISITION AND ANALYSIS OF WHEEL WEAR DATA

The measuring instruments currently available for wheel-rail wear can be classified into contact and non-contact types according to the measurement method. Non-contact instruments, such as the OPTIMESS laser sensing system [33] and CALIPRIC laser device for wheel and rail profile measurement [34], feature high efficiency and precision, but at a high cost. Contact instruments, such as the Danmark MiniProf series profile-measuring instrument [35], allow for easy operation at a lower cost, but they require a larger amount of work and their precision is relatively low.

In this study, a non-contact measuring instrument was used to measure the wheel wear, and a method based on pattern search was adopted to improve the measurement accuracy and correct the position deviation. Figure 3 shows this instrument.

The curve deviation F is a function involving three independent variables: the coordinate axis's lateral movement X,

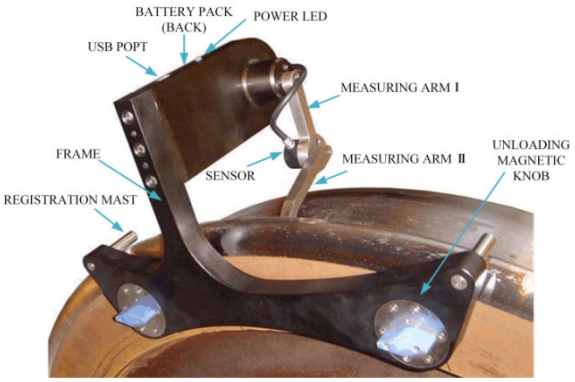

FIGURE 3. Wheel profile measuring equipment.

longitudinal movement Y, and rotation relative to the coordinate origin *alpha*. Assuming that the post-wear curve is composed of n scatter points, the curve deviation $F(X, Y, alpha)$ is expressed as follows:

$$F(X, Y, alpha) = \sum_{k=1}^{n} (\|d_k\|)/n, \tag{2}$$

where d_k indicates the distance between two adjacent points on the post-wear and pre-wear curves [36], [37]. A pattern search method (Hooke–Jeeves) [38], [39] was applied to calculate a set of optimal values (*X, Y, alpha*) and minimize the deviation between the two curves F (*X, Y, alpha*).

B. OPTIMIZATION OF WEAR COEFFICIENT BASED ON GENETIC ALGORITHM

In a genetic algorithm, the independent variable is regarded as the organism, and the optimized objective function is defined as the fitness based on the basic principle of biogenetics during parameter optimization [40]. The unknown function is regarded as the living environment. The global optimal solution is finally found through repetitive iterations [41].

Given the actual track and operating speed, 50,000 km measured data were obtained. The Jendel wear model was compiled using Matlab and the wheel wear was calculated using k. The linear regression theory and least-squares algorithm [42] were used to determine the difference between the measured and simulated wear values, and the minimum difference was regarded as the objective function for the optimization of coefficient k.

Assume $\{(X_i, Y_i)\}$ $(i = 1, 2, \ldots, m)$ in which X_i represents the measured wheel profile data and Y_i is the wear value simulated with k. The difference between the two data sets is denoted E. Ensure that $Y_i(k) \in \Psi$ is within the defined function class Ψ. The squared difference can be formulated as

$$E^2 = \sum_{i=1}^{m} [X_i - Y_i(k)]^2, \tag{3}$$

Here, E^2 is regarded as the objective function. The algorithmic mechanism is presented in Figure 4.

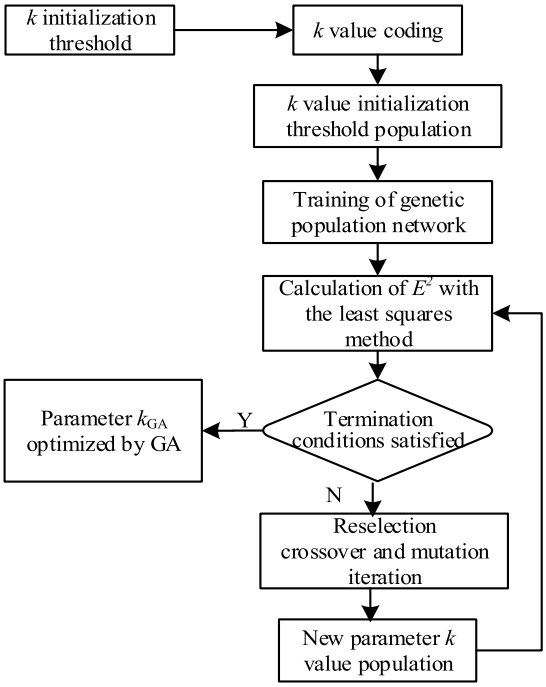

FIGURE 4. Genetic algorithm-based calculation process.

For the decision variable k, the initialization threshold consists of the upper and lower bounds of the Jendel model in different zones. The genetic algorithm population refers to different areas of the Jendel wear model. Various k values were determined for different ranges of sliding speed and contact pressure. The algorithm constraint consists of the updated mileage and the threshold for smoothing.

Call the GA function [x, fval, exitflag] = ga (ObjectiveFunction, nvars, [], [], [], [], LB, UB) in Matlab, where the main parameters are as follows:

x is the best point that GA locates during its iterations, namely the optimal solutions for k, including k_1, k_2, and k_3. fval is fitness function evaluated at x. exitflag is Integer giving the reason GA stops iterating. ObjectiveFunction is handle to the fitness function. The fitness function should accept a row vector of length nvars and return a scalar value. nvars is positive integer representing the number of variables in the problem. nvars = 3. LB is the lower bound of k, i.e. $k_1 = 1 \times 10^{-4}$, $k_2 = 30 \times 10^{-4}$, and $k_3 = 1 \times 10^{-4}$. UB is the upper bound of k, i.e. $k_1 = 10 \times 10^{-4}$, $k_2 = 40 \times 10^{-4}$, and $k_3 = 10 \times 10^{-4}$.

The lengths of all track segments and operating speeds were input into the software Matlab for optimization of the wear coefficient k. The vehicle dynamics, wheel-rail contact, and the optimized Jendel wear models were combined to predict wheel wear.

C. OPTIMIZATION OF WEAR COEFFICIENT BASED ON PARTICLE SWARM OPTIMIZATION

Both particle swarm optimization (PSO) and genetic algorithm (GA) belong to the class of bio-inspired optimization

algorithms [43]. They have many similarities, such as in algorithmic mechanism and implementation. PSO requires fewer codes and parameters than GA. Compared to traditional algorithms, PSO shows much faster computational speed and greater global search capability.

With good optimization performance, PSO was used to optimize the wear coefficient k (k_1, k_2, k_3). If a particle can minimize the difference between simulated and measured values, this particle's position is considered the optimal k value found. In this paper, particle's velocity and position are updated by fitness function for PSO, which is defined as the difference between simulated and measured values.

Figure 5 presents the flow chart of PSO.

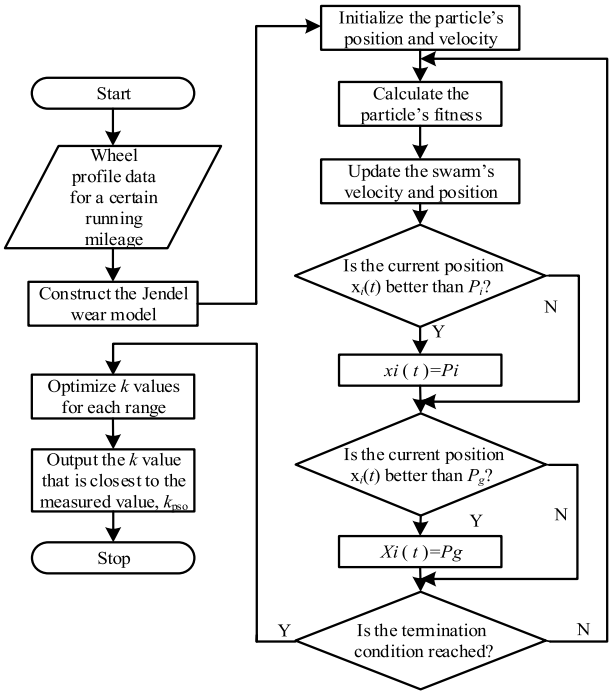

FIGURE 5. Flow chart of PSO.

The specific steps of the algorithm are as follows:

1) Initialization of PSO parameters: randomly set the initial position x_i and initial velocity v_i of particle i, which are given by

$$x_i = (x_{i,1}, x_{i,2}, x_{i,3}, \ldots, x_{i,d}), \tag{4}$$

$$v_i = (v_{i,1}, v_{i,2}, v_{i,3}, \ldots, v_{i,d}), \tag{5}$$

where i indicates particle's serial number; d is the number of spatial dimensions where particle i is located; and $x_{i,d}$ and $v_{i,d}$ are the position and velocity, respectively, of particle i in d dimensions.

Set the value range for parameter k (k_1, k_2, k_3). The lower bounds: $k_1 = 1 \times 10^{-4}$, $k_2 = 30 \times 10^{-4}$ and $k_3 = 1 \times 10^{-4}$; the upper bounds: $k_1 = 10 \times 10^{-4}$, $k_2 = 40 \times 10^{-4}$ and $k_3 = 10 \times 10^{-4}$. Set the learning factors: $c_1 = c_2 = 2$. The initial number of particle swarms is set at 40. Initialize the number of dimensions of the swarms, d, to 3. Set the number of iterations t at 30 and the inertia weight w at between 0.5-1.2.

2) Calculate the fitness of each particle, f_{ness}, and let the current position of particle i, denoted P_i, be its best position. Then the swarm's best position, P_g, can be determined by comparing the fitness of all particles in the swarm.

3) In each iteration, each particle updates itself by tracking the optimal solution found by itself and the optimal solution found by the whole swarm.

$$v_{i,d}(t+1) = wv_{i,d} + c_1 r_1 (P_{i,d} - x_{i,d}(t)) + c_2 r_2 (P_{g,d} - x_{i,d}(t)), \tag{6}$$

$$x_{i,d}(t+1) = x_{i,d}(t) + v_{i,d}(t+1), \tag{7}$$

where $P_{i,d}$ represents the best historical position of particle i; $P_{g,d}$ represents the best historical position of the whole swarm; and r_1 and r_2 are uniformly distributed random numbers between 0 and 1.

4) Return to step 2) and repeat the iterative optimization using the updated position and velocity of the particle. If x_i (t) $\geq P_i$, then x_i (t) $= P_i$; if x_i (t) $\geq P_g$, then x_i (t) $= P_g$. Continuously update P_i and P_g until the maximum number of iterations is reached. Then the search process stops and the optimal k value is output.

D. OPTIMIZATION OF WEAR COEFFICIENT BASED ON TABU SEARCH

Tabu Search (TS) is a heuristic search method that extends neighborhood for progressive global optimization. It employs the "prohibitions" technique to expand search space, which involves preventing repetition of previous work and finding new neighborhood using the memory stored in a Tabu Search list. TS has been widely studied and applied to production since it was created in the 1980s [44], [45]. Its optimization efficiency and results are closely associated with algorithm design.

TS was implemented to optimize the wear coefficient. The objective function is the same as in the GA process. The lower bounds of k are as follows: $k_1 = 1 \times 10^{-4}$, $k_2 = 30 \times 10^{-4}$ and $k_3 = 1 \times 10^{-4}$; the upper bounds: $k_1 = 10 \times 10^{-4}$, $k_2 = 40 \times 10^{-4}$ and $k_3 = 10 \times 10^{-4}$. The initial point k_0 is generated randomly between the lower and upper bounds. The number of neighboring solutions, denoted Ca, is set to 5. The tabu length, L, is an integer between 5 and 11. The initial value for adaptive weight coefficient, w, is 1. The search radius is reduced by 0.2% every time the tabu list is updated. The maximum number of iterations, G, is set to 200. The optimal solution found by Tabu Search is denoted k (k_1, k_2, k_3).

Figure 6 shows the flow chart of Tabu Search.

E. OPTIMIZATION OF WEAR COEFFICIENT BASED ON SIMULATED ANNEALING

Simulated Annealing (SA) is a classical natural computing algorithm using physical analogy. It starts with improvement in the local search algorithms and simulates the slow cooling

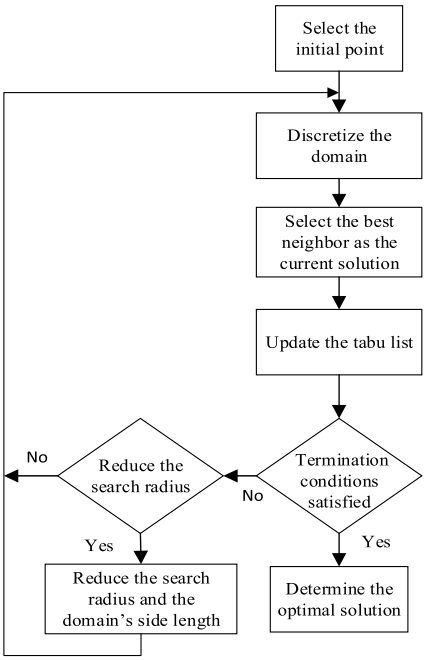

FIGURE 6. Flow chart of Tabu Search.

(annealing) of a metal after heating until the metal system reaches a state with minimum energy (solid at room temperature). This algorithm tries to find a global optimum for the optimization problem [46].

In SA, the objective function for the optimization problem is analogous to the energy of the metal system and the Metropolis criterion is reasonably introduced to determine whether to accept the new solution. Assume $\min_{i\in S} f(i)$ an optimization problem $\min_{i\in S} f(i)$, and let S represent a set of feasible solutions for the objective function f(i). If a new solution j is generated from the current solution i, whether j should be accepted as the current solution will be decided based on transition probability, which is defined as

$$P_i(i \Rightarrow j) = \begin{cases} 1, & \text{if } f(j) < f(i) \\ \exp(\dfrac{f(i) - f(j)}{T}), & \text{or,} \end{cases} \quad (8)$$

where T is a control parameter representing the metal system's temperature. Normally, T takes a large value, T_0 (corresponding to heating), at the beginning, and then it declines slowly (corresponding to slow cooling) to $T_k (k = 1, 2, \ldots\ldots)$. For each T_k value, the Metropolis criterion is implemented L_k times. Then T transitions to the next control parameter T_{k+1}. This process seeks to find potential regions for search by fully simulating the thermal motion of molecules [47].

Call the SA function simulannealbnd from the Global Optimization Toolbox in MATLAB:

x = simulannealbnd (ObjectiveFunction, x_0, LB, UB);

Input parameters include ObjectiveFunction, x_0, LB, and UB, with ObjectiveFunction being the same objective function as that used in GA. x_0, the initial value, is set as follows: $k_1 = 5 \times 10^{-4}$, $k_2 = 35 \times 10^{-4}$ and $k_3 = 5 \times 10^{-4}$. LB is the lower bound of k: $k_1 = 1 \times 10^{-4}$, $k_2 = 30 \times 10^{-4}$, and $k_3 = 1 \times 10^{-4}$. UB is the upper bound of k: $k_1 = 10 \times 10^{-4}$, $k_2 = 40 \times 10^{-4}$, and $k_3 = 10 \times 10^{-4}$. The output parameter x is the optimum found, i.e. the optimal values for wear coefficient k (k_1, k_2, k_3).

V. PHYSICAL MODEL FOR WHEEL WEAR PREDICTION

Developed by the German company INTEC Gmbh (officially renamed SIMPACK AG in 2009), SIMPACK is a multibody dynamics analysis software package for kinetic/dynamic analysis of any mechanical or electromechanical system. With high computational accuracy and stability, it has been applied for years by many colleges and universities, as well as companies like BMW and Siemens.

In this paper, SIMPACK was used to create physical models for wheel wear prediction. These models include a vehicle-track multi-body dynamics model, wheel-rail contact model, optimized Jendel wear model, and wheel profile upgrading model. The vehicle-track dynamics model was used to calculate the spatial geometry of wheel-rail contact. The wheel-rail contact model was applied for further detailed calculation of the wheel-rail contact patch, creep force distribution and other parameters. The calculation results from the wheel-rail contact model were then input into the optimized Jendel wear model to calculate the unit volume of wheel wear. After the vehicle travels a certain distance, the profile of each wheel will change. So the wheel profile upgrading model was applied to generate a new wheel profile, which was then input into the vehicle dynamics model to for repeated calculations of wheel wear.

A. VEHICLE-TRACK MULTI-BODY DYNAMICS MODEL

According to the Chinese general standard, urban rail vehicles in China are classified into five types: A, B, C, D, and L (B2). The primary distinguishing factor between the five types is vehicle width. Type B metro vehicles, each measuring 19 m long and 2.8 m wide, were studied in this paper.

A multi-body dynamics model of a single vehicle system was developed for type B metro vehicle. In this model, the vehicle body, framework, motor, gear drive unit, axle box, and wheel set are multi-DOF rigid bodies; the axle box spring, air spring, oil damper, anti-roll bar, rubber joint, and lateral stop are simplified as functional expressions of force.

In order to ensure the accuracy of the models, all modeling parameters used in the study were obtained from actual measurements. Table 1 displays the values of some parameters.

In Table 1, AW0 indicates the load of an empty metro vehicle. AW1 indicates metro vehicle load when passengers are full of seats. AW2 indicates the load of the metro vehicle with six passengers per square meters. AW3 indicates the load of the metro vehicle with nine passengers per square meters.

Lines consist of straight lines and curves, and actual track conditions are shown in Table 1. In order to simulate different operating environments, the curves are designed as S-curve. The S-curve, also known as continuously turning

TABLE 1. Actual parameters of several vehicles.

Vehicle body load on line ① (the characteristics of actual passenger flow are considered)			
AW1 accounting for 75%	AW2 accounting for 20%	AW3 accounting for 5%	Load applied in modeling 100%
22 t	33.9 t	39.9 t	25.3 t
Actual track conditions for lines ① and ②			
Track radius (R)		Track proportion	Running speed
R > 1, 200 m		75%	70 km/h
R800 m to R1, 200 m		11%	70 km/h
R600 m to R800 m		11%	60 km/h
R350 m to R600 m		3%	40 km/h
Vehicle body load on line ② (the characteristics of actual passenger flow are considered)			
AW0 accounting for 20%	AW2 accounting for 50%	AW3 accounting for 30%	Load applied in modeling 100%
19 t	33.9 t	39.9 t	32.7 t
Actual wheel-rail parameters for lines ① and ②			
Track excitation (line ①)	AAR 5	Track excitation (line ②)	German spectrum
Tread profile	LM	Material Poisson's ratio	0.3
Friction coefficient	0.4	Rail cant	1:40
Rail type	60 kg/m	Wheel diameter	840 mm
Parameters of type B metro vehicle			
Wheel set mass	1018 kg	Vertical stiffness of primary spring	1.3 MN/m
Axle box mass	110 kg	Longitudinal damping of axle box joint	5620 N·s/m
Frame mass	2103 kg	Secondary vertical damping	25 kN·s/m
Bogie wheelbase	2300 mm	Secondary lateral damping	58 kN·s/m
Length between bogie centers	12600 mm	Maximum running speed	80 km/h

curve, represents a track line composed of two continuous circular segments and an easement curve linking them. The two circular segments have the same radius and length but bend in opposite directions, with one bending to the left and the other to the right. Figure 7 shows the schematic of the S-curve.

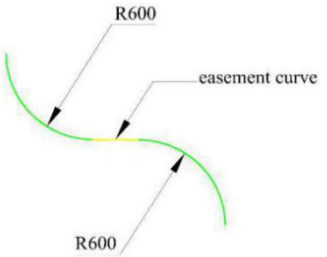

FIGURE 7. Schematic of S-curve.

The dynamics model and its topological graph are illustrated in Figure 8.

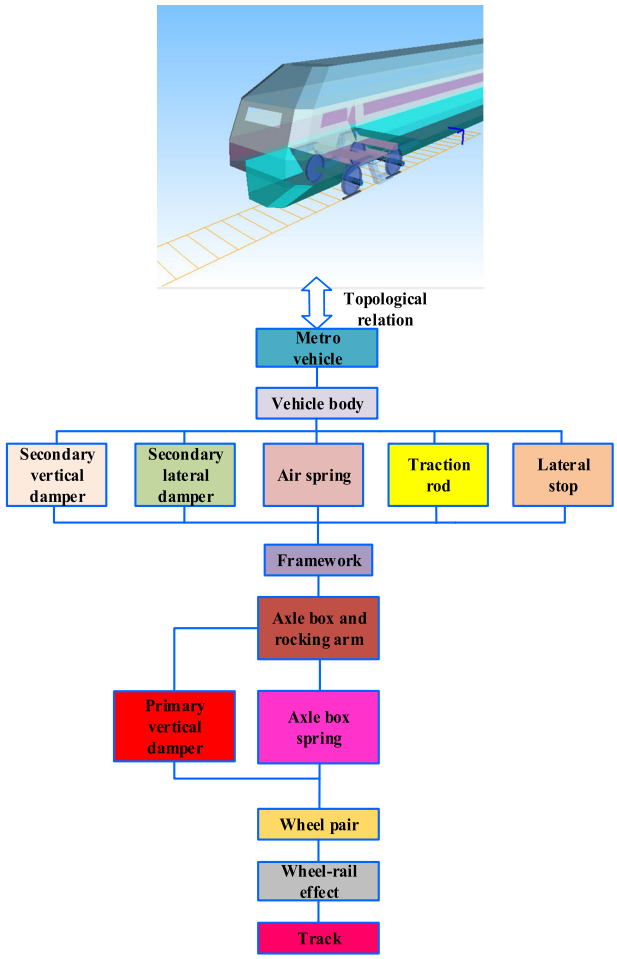

FIGURE 8. Vehicle-track dynamics model and its topological graph.

The vehicle dynamics model was used to calculate the spatial geometry of wheel-rail contact, and then determine the position of the wheel-rail contact patch, approximate shape of the elliptical contact patch, and sum of external forces acting on the contact patch, accordingly.

B. WHEEL-RAIL CONTACT MODEL

Furthermore, the wheel-rail contact model was applied to calculate the shape of the wheel-rail contact patch, creep force distribution, and stick-slip area distribution in detail.

The wheel-rail contact normal force was calculated based on the Hertzian contact theory, which is illustrated in Figure 9 [48].

The theory holds that the contact patch between the two elastic bodies is elliptical in shape, and the curvature of two objects within the contact patch is constant. The normal gap between the two elastic bodies can be expressed as follows:

$$\Delta z(x, y) = A_1 x^2 + A_2 y^2, \tag{9}$$

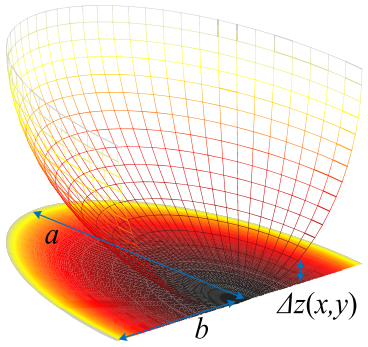

FIGURE 9. Hertzian contact theory-based elastomer contact effect.

where A_1 and A_2 are the relative curvatures; and x and y indicate the longitudinal and transverse coordinates, respectively.

The two half axes of the elliptical contact patch, a and b, are given by

$$\begin{cases} a = m_1 \left[\dfrac{3\pi N(k_A + k_B)}{4(A_1 + A_2)} \right]^{1/3} \\ b = m_2 \left[\dfrac{3\pi N(k_A + k_B)}{4(A_1 + A_2)} \right]^{1/3} \end{cases}, \tag{10}$$

where m_1 and m_2 indicate the Hertzian contact coefficients; N denotes the normal load; and k_A and k_B are constants. The normal force is calculated as follows:

$$p_z(x, y) = \frac{3N}{2\pi ab} \sqrt{1 - (\frac{x}{a})^2 - (\frac{y}{b})^2}. \tag{11}$$

To solve the wheel-rail tangential contact problem, the contact patch was divided into stick-slip areas based on the solution to the normal contact problem; that is, the contact patch was divided into stick and creep areas to solve the creep force distribution in the contact patch. In this study, the FASTSIM algorithm [49] based on Kalker's simplified theory of rolling contact was applied to determine the tangential force.

In the 1960s, Kalker proposed the Linear Theory to examine creep force - creepage relationship and the spin effect was also considered in this model. Using the traction-displacement relationship based on the general elastic theory and integrating the traction over the contact area, the tangential force $F_T = [F_x \ F_y]^{\mathbf{T}}$ and the torsion couple M can be expressed as linear functions of the creepages and spin:

$$\begin{bmatrix} F_x \\ F_y \\ M \end{bmatrix} = -Gab \begin{bmatrix} C_{11} & 0 & 0 \\ 0 & C_{22} & \sqrt{ab}C_{23} \\ 0 & -\sqrt{ab}C_{23} & abC_{33} \end{bmatrix} \begin{bmatrix} \xi_x \\ \xi_y \\ \varphi \end{bmatrix}, \tag{12}$$

where a and b are two half axes of the elliptical contact patch in the rolling direction and lateral direction; C_{ij} are the Kalker's coefficients; G is the material's shear modulus; ξ_x, ξ_y, φ denote the longitudinal, transverse, and spin creep rates, respectively.

The Simplified Theory of rolling contact is generally applied in wheel-rail contact calculation where the contact area is elliptic [50]. By using the so-called compliant parameters in the longitudinal and lateral directions (L_x and L_y), the complex expression derived from the general elastic theory can be simplified. The compliant parameters depend on the creepage and spin coefficients in linear theory. The tangential forces $F_T = [F_x \ F_y]^{\mathbf{T}}$ and tangential surface displacement u^{wr} are related by the following equation:

$$u^{\mathrm{wr}} = u^{\mathrm{w}} - u^{\mathrm{r}} = \begin{bmatrix} L_x F_{Tx} & L_y F_{Ty} \end{bmatrix}^{\mathbf{T}}. \tag{13}$$

The tangential forces are determined by integrating over the contact area:

$$F_x = \int_{-b}^{b} \int_{-a}^{a} F_{Tx} dxdy = -\frac{8a^2 b\xi_x}{3L_x}, \tag{14a}$$

$$F_y = \int_{-b}^{b} \int_{-a}^{a} F_{Ty} dxdy = -\frac{8a^2 b\xi_y}{3L_y} - \frac{\pi a^3 b\varphi}{4L_y}, \tag{14b}$$

The compliant parameters are obtained by equating equations 12 and 14 as follow:

$$\begin{cases} L_x = \dfrac{8a}{3GC_{11}} \\ L_y = \dfrac{8a}{3GC_{22}} \\ L_{y2} = \dfrac{\pi a^2}{4G\sqrt{ab}C_{23}}. \end{cases} \tag{15}$$

The FASTSIM algorithm based on the simplified theory of rolling contact is extensively applied in railroad computer programs. This theory can help to reduce the calculation time significantly with the application of the compliant parameters.

C. WEAR CALCULATION AND TREAD UPGRADING

The calculation results from the wheel-rail contact model were input into the optimized Jendel wear model. Then equation (1) in Section III was used to calculate wheel wear and the wear depth distribution on the wheel profile. The wear coefficient in equation (1) takes optimized values.

Given that wheel profile will change due to wear after the vehicle travels a certain distance, a profile upgrading model was implemented to upgrade wheel profile and the new profile was then input into the vehicle-track dynamics model for every 5000 km traveled to allow for cyclic calculation. First, the cubic spline interpolation algorithm for smoothing was used to provide post-wear wheel profile. The new profile was input into SIMPACK to upgrade the original profile. In this way, the wheel wear was calculated cyclically until the running mileage reached a specified distance.

VI. COMPARISON OF SIMULATED AND MEASURED WEAR DATA

A. COMPARISON OF SIMULATED AND MEASURED DATA FOR LINE ①

Wheel wear for 50,000 and 80,000 km were measured on metro line ① in X, a Chinese city with a population of about 10 million. The data are illustrated in Figure 10.

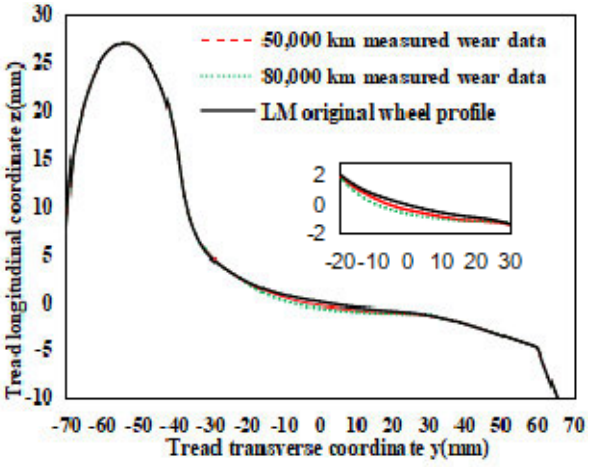

FIGURE 10. 50,000 and 80,000 km wear measurements for Line ①.

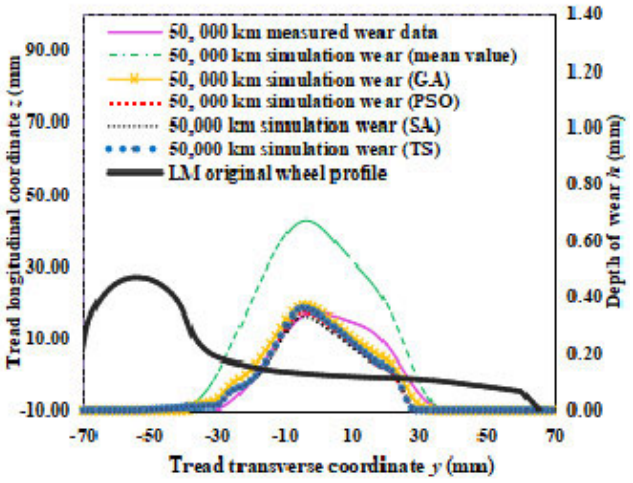

FIGURE 11. Comparison between predicted and measured wheel wear for 50,000 km on line ①.

1) The traditional wear simulation principle based on the physical model was adopted, and mean values determined for the Jendel model's wear coefficients are as follows: $k_1 = 5 \times 10^{-4}$, $k_2 = 35 \times 10^{-4}$, and $k_3 = 5 \times 10^{-4}$. Finally, wheel wear simulation was conducted with the mean k values.
2) Based on the analysis of the measured wear data for 50,000 km, the wear coefficient k was optimized using the genetic algorithm. The optimized k values, including $k_{1G} = 2.547 \times 10^{-4}$, $k_{2G} = 36.298 \times 10^{-4}$, and $k_{3G} = 8.855 \times 10^{-4}$, were then used for the wheel wear simulation.
3) Based on the analysis of the measured wear data for 50,000 km, the wear coefficient k was optimized using the PSO. The resulting k values, including $k_{1P} = 2.371 \times 10^{-4}$, $k_{2P} = 38.258 \times 10^{-4}$, and $k_{3P} = 5.845 \times 10^{-4}$, were used for the wheel wear simulation.
4) Based on the analysis of the measured wear data for 50,000 km, the TS was adopted for optimization of the wear coefficient k. The resulting k values, including $k_{1T} = 2.476 \times 10^{-4}$, $k_{2T} = 36.033 \times 10^{-4}$, and $k_{3T} = 1.000 \times 10^{-4}$, were then used for the wheel wear simulation.
5) The SA was also adopted for optimization of the wear coefficient k based on the measured wear data for 50,000 km. The resulting k values, including $k_{1S} = 2.354 \times 10^{-4}$, $k_{2S} = 36.647 \times 10^{-4}$, and $k_{3S} = 3.564 \times 10^{-4}$, were then used to simulate the wheel wear.

Figure 11 provides a comparison between the predicted and measured wheel wear for 50,000 km on line ①.

It is clear from Figure 11 that under other identical modeling conditions, a large error exists between the simulated wear depth (with the mean value k) and the measured value, which implies that it is impossible to simulate the degree of wear accurately by the traditional method. By comparison, the wear predictions for 50,000 km obtained by GA, PSO, TS and SA are close to the measurements. The accurate simulation of wheel wear verifies the accuracy of this method.

6) The Jendel wear model that takes the mean value of the wear coefficient was usedto calculate and predict the wheel wear for 80,000 km.
7) The Jendel wear model with the wear coefficient optimized by genetic algorithm ($k_{1G} = 2.547 \times 10^{-4}$, $k_{2G} = 36.298 \times 10^{-4}$, and $k_{3G} = 8.855 \times 10^{-4}$) was used to calculate and predict the wheel wear for 80,000 km.
8) The Jendel wear model with k values optimized by PSO($k_{1P} = 2.371 \times 10^{-4}$, $k_{2P} = 38.258 \times 10^{-4}$, and $k_{3P} = 5.845 \times 10^{-4}$) was used for wear calculation and prediction.
9) The Jendel wear model with k values optimized by TS($k_{1T} = 2.476 \times 10^{-4}$, $k_{2T} = 36.033 \times 10^{-4}$, and $k_{3T} = 1.000 \times 10^{-4}$) was used for wear calculation and prediction.
10) The Jendel wear model with k values optimized by SA ($k_{1S} = 2.354 \times 10^{-4}$, $k_{2S} = 36.647 \times 10^{-4}$, and $k_S = 3.564 \times 10^{-4}$) was used for wear calculation and prediction.

The prediction results are illustrated in Figure 12. As shown in the figure, the 80,000 km wheel wear was accurately predicted using the GA, PSO, TS and SA, but the result obtained by the traditional method with the mean k value significantly exceeded the measured wea. Thus, optimization of the k value by means of the GA, PSO, TS and SA can make the predictions closer to the measurements.

B. LINE ② METRO WHEEL MEASUREMENT AND SIMULATION RESULTS

The generalization ability of this method was further verified through comparison with the wheel wear data for 140,000 km measured on line ②, as illustrated in Figure 13.

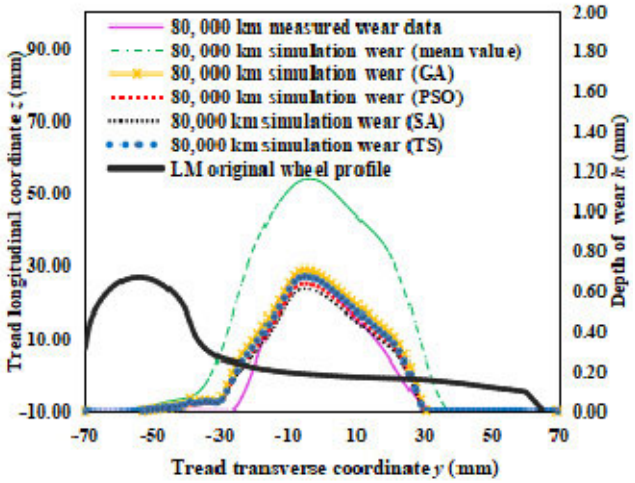

FIGURE 12. Comparison between predicted and measured wheel wear for 80,000 km on line ①.

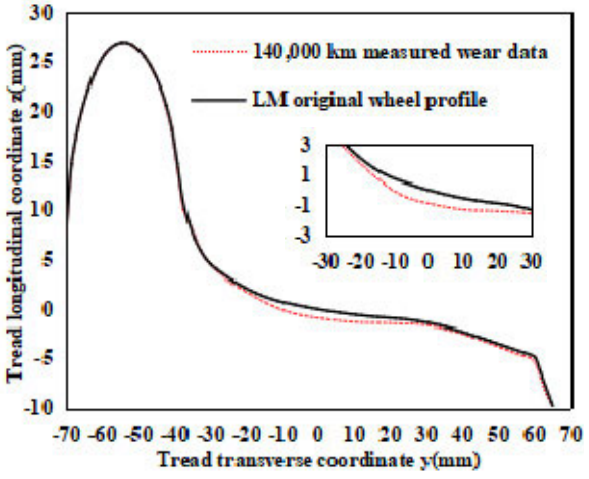

FIGURE 13. 140,000 km wear measurement from line ② metro wheels.

Mean values were determined for the Jendel model's wear coefficients: $k_1 = 5 \times 10^{-4}$, $k_2 = 35 \times 10^{-4}$, and $k_3 = 5 \times 10^{-4}$.

The optimized k values determined by GA are as follows: $k_{1G} = 3.715 \times 10^{-4}$, $k_{2G} = 36.407 \times 10^{-4}$, and $k_{3G} = 8.180 \times 10^{-4}$.

The k values optimized by PSO: $k_{1P} = 3.744 \times 10^{-4}$, $k_{2P} = 33.194 \times 10^{-4}$, and $k_{3P} = 8.065 \times 10^{-4}$.

The k values optimized by TS: $k_{1T} = 3.667 \times 10^{-4}$, $k_{2T} = 30.000 \times 10^{-4}$, and $k_{3T} = 10.000 \times 10^{-4}$.

The k values optimized by SA: $k_{1S} = 3.642 \times 10^{-4}$, $k_{2S} = 34.057 \times 10^{-4}$, and $k_{3S} = 1.877 \times 10^{-4}$.

The mean k and optimized k values were used separately for the 140,000 km wear simulation. The results are illustrated in Figure 14.

As indicated in the figure, the 140,000 km wheel wear predicted using mean values of k deviated significantly from the measured result, while less error existed between the

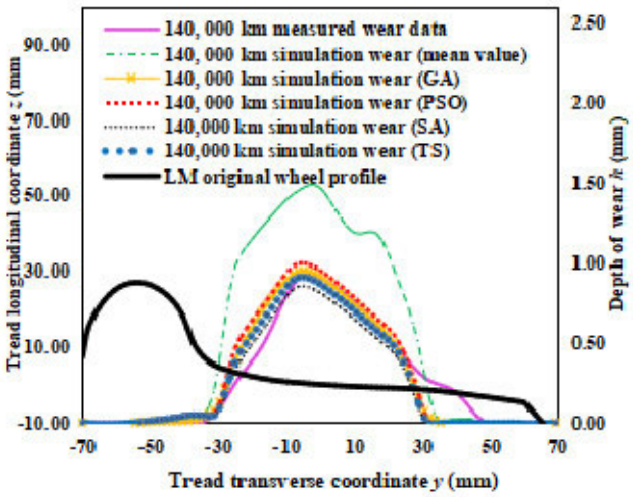

FIGURE 14. Comparison between wheel wear predictions and measurements for 140,000 km on line ②.

simulation result and the measured wheel profile when the optimized k value was adopted, which suggest a more accurate wheel wear prediction.

The updating process of wheel wear calculation described above is based on the following assumption: with adequate operating mileage, the cumulative growth in wheel wear within a short distance is linear. The pattern of linear growth is determined by the unary linear regression relation of the unit wear in the Jendel model to wear coefficient k and normal force N, and the unary linear regression relation between the sliding speed and wheel pair lateral displacement. A comparison with the measured data verifies the effectiveness of the proposed method.

C. PERFORMANCE COMPARISON BETWEEN TRADITIONAL METHOD AND OPTIMIZATION ALGORITHMS

The results produced by the traditional method and the four optimization algorithms are compared based on root-mean-square error in wear value, maximum wear depth, relative error in maximum wear depth and optimization time (Table 2).

Root-mean-square error (RMSE) is a good measure of measurement accuracy. It is calculated by summing the squares of the differences between measured values, $X_{measured,i}$, and simulated values, $X_{\text{simulated},i}$, and then taking the square root of the ratio of the sum to the number of observations, $n_{measured}$, [51]:

$$RMSE = \sqrt{\frac{\sum_{i=1}^{n} (X_{measured} - X_{simulated})^2}{n_{measured}}}, \qquad (16)$$

Maximum wear depth is usually a key quantity considered in relevant research. A wheel will need turning repair if the maximum wear depth in it exceeds a certain limit.

Relative error in maximum wear depth refers to the ratio of the absolute error in wear prediction to measured wear and is

TABLE 2. Comparison Of the results produced by traditional method and optimization algorithms.

Line and running mileage	Different calculation methods	RMSE	Maximum wear depth $X_{max\ dep}$ (mm)	$RE_{max\ depth}$	Computation time (s)
50,000 km on line ①	Measured data	0	0.348	0	——
	Traditional method	0.1627	0.673	93.4%	——
	GA	0.0303	0.372	6.9%	2117
	PSO	0.0376	0.349	0.3%	212
	TS	0.0349	0.362	4.0%	778
	SA	0.0399	0.333	-4.3%	634
80,000 km on line ①	Measured data	0	0.683	0	——
	Traditional method	0.3313	1.167	70.9%	——
	GA	0.0700	0.710	3.9%	——
	PSO	0.0462	0.642	-6.0%	——
	TS	0.0520	0.677	-0.9%	——
	SA	0.0469	0.614	-10.1%	——
140,000 km on line ②	Measured data	0	0.929	0	——
	Traditional method	0.3711	1.488	60.2%	——
	GA	0.0947	0.9477	2.0%	2537
	PSO	0.1095	0.9965	7.3%	615
	TS	0.0915	0.9090	-2.2%	799
	SA	0.0935	0.8526	-8.2%	1330

expressed as a percentage. It is given by the formula below:

$$RE_{\max\ depth} = \frac{X_{simulated,\max\ dep} - X_{measured,\max\ dep}}{X_{measrued,\max\ dep}} \times 100\%, \tag{17}$$

where $RE_{\max\ depth}$ is the relative error in maximum wear depth; $X_{\text{measured, maxdep}}$ is the measured maximum wear depth; and $X_{\text{simulated, maxdep}}$ represents the maximum wear depth simulated by the traditional method and optimization algorithms.

As shown in Table 2, the values predicted by the optimization algorithms are closer to the measured values than the results of the traditional method. The RMSE in the predictions from the four optimization algorithms are significantly lower than the RMSE in the values calculated by the traditional method. In particular, TS outperforms other algorithms for both lines.

In terms of the relative error in maximum wear depth, the relative errors between the wear predictions by the optimization algorithms and measured wear are smaller than 11%, while the relative errors between the results of traditional methods and measurement exceeds 60%. A comparison of the results for the two lines suggests that TS has the best performance.

From the perspective of computation time, GA requires the longest computation time, while PSO demonstrates the highest efficiency.

VII. CONCLUSION

Integrated data-model-driven approach combines the advantages of data-driven and model-based methods while avoiding their disadvantages. Data-model-driven integration was applied to simulation and prediction of metro wheel wear, in order to improve the accuracy of prediction and reduce data costs. A parameter in the physical model was optimized, with the wear data for a certain running mileage used as the sample. The optimized physical model allows for more accurate simulation and prediction of metro wheel wear for other running mileage. A comparison between traditional method and the optimization algorithms used in this study suggests that the data-model-driven integration improves the accuracy and efficiency of metro wheel wear prediction, reduces the experimental cost, and offers a new approach to wheel wear research.

The model parameter was optimized using Genetic Algorithm (GA), Particle Swarm Optimization (PSO), Tabu Search (TS) and Simulated Annealing (SA), separately. The four optimization algorithms produced generally consistent results and show high performance.

There are many other intelligent optimization algorithms, such as differential evolution algorithms, immune algorithms, ant colony optimization algorithms, and neural network algorithms. In future work, these optimization algorithms will be studied and compared with the current algorithms. Moreover, more research will be conducted on the application of machine learning methods in wheel wear prediction.

ACKNOWLEDGMENT

The authors are grateful to the anonymous reviewers for providing insightful comments aimed at improving the paper.

REFERENCES

[1] Z. Liu, Z. Jia, C. Vong, J. Han, C. Yan, and M. Pecht, "A patent analysis of prognostics and health management (PHM) innovations for electrical systems," *IEEE Access*, vol. 6, pp. 18088–18107, 2018.
[2] D. Zhang, L. Qian, B. Mao, C. Huang, B. Huang, and Y. Si, "A data-driven design for fault detection of wind turbines using random forests and XGboost," *IEEE Access*, vol. 6, pp. 21020–21031, 2018.
[3] U. Iqbal, T. Y. Wah, M. H. U. Rehman, and M. Qurat-Ul-Ain, "Usage of model driven environment for the classification of ECG features: A systematic review," *IEEE Access*, vol. 6, pp. 23120–23136, 2018.
[4] S. Morando, S. Jemei, D. Hissel, R. Gouriveau, and N. Zerhouni, "ANOVA method applied to proton exchange membrane fuel cell ageing forecasting using an echo state network," *Math. Comput. Simul.*, vol. 131, pp. 283–294, Jan. 2017.
[5] J. L. Godwin, "Exploiting robust multivariate statistics and data driven techniques for prognosis and health management," Ph.D. dissertation, Eng. Com., Durham Univ., Durham, U.K., 2015.
[6] A. Cubillo, "Physics-based approach to detect metal-metal contact in the hydrodynamic bearing of a planetary transmission," Ph.D. dissertation, SATM, Cranfield Univ., Cranfield, U.K., 2016.

[7] M. Ibrahim, N. Y. Steiner, S. Jemei, and D. Hissel, "Wavelet-based approach for online fuel cell remaining useful lifetime prediction," *IEEE Trans. Ind. Electron.*, vol. 63, no. 8, pp. 5057–5068, Aug. 2016.

[8] P. Tamilselvan and P. F. Wang, "Failure diagnosis using deep belief learning based health state classification," *Rel. Eng., Syst. Safety*, vol. 115, pp. 124–135, Jul. 2013.

[9] C. Li, R.-V. Sanchez, G. Zurita, M. Cerrada, D. Cabrera, and R. E. Vásquez, "Gearbox fault diagnosis based on deep random forest fusion of acoustic and vibratory signals," *Mech. Syst. Signal Process.*, vol. 76, pp. 283–293, Aug. 2016.

[10] A. Peimankar, S. J. Weddell, T. Jalal, and A. C. Lapthorn, "Multi-objective ensemble forecasting with an application to power transformers," *Appl. Soft Comput.*, vol. 68, pp. 233–248, Jul. 2018.

[11] M. Malinowski, "Harmonizing prognostics and health management with risk analysis for smart manufacturing systems," M.S. thesis, SEAS, Univ. Virginia, Charlottesville, VA, USA, 2016.

[12] Z. Liu, "Cyber-physical system augmented prognostics and health management for fleet-based systems," Ph.D. dissertation, Eng. App., Univ. Cincinnati, Cincinnati, OH, USA, 2018.

[13] G. Kan, "Study on application and comparison of data-driven model and semi-data-driven model for rainfall-runoff simulation," *Acta Geodaetica Et Cartographica Sinica*, vol. 46, no. 2, p. 265, Feb. 2017.

[14] X.-R. Fan, M.-Z. Kang, E. Heuvelink, P. de Reffye, and B. G. Hu, "A knowledge-and-data-driven modeling approach for simulating plant growth: A case study on tomato growth," *Ecolog. Model.*, vol. 312, pp. 363–373, Sep. 2015.

[15] M. Baptista, S. Sankararaman, I. P. de Medeiros, C. Nascimento, Jr., H. Prendinger, and E. M. P. Henriques, "Forecasting fault events for predictive maintenance using data-driven techniques and ARMA modeling," *Comput. Ind. Eng.*, vol. 115, pp. 41–53, Jan. 2018.

[16] L. Wang, H. Yuan, W. B. Na, X. A. Chen, and Y. T. Li, "Optimization of the re-profiling strategy and remaining useful life prediction of wheels based on a data-driven wear model," *Syst. Eng.-Theory Pract.*, vol. 31, no. 6, pp. 1143–1152, 2011.

[17] Z. Yang, Z. Xing, L. Wang, and J. Long, "Optimization of wheel re-profiling strategy based on statistical wear model," *Railway Standard Des.*, vol. 99, no. 1, pp. 142–148, 2018.

[18] Ž. Dordević, M. Vasiljević, S. Vesković, S. Rajilić, and V. Vukadinović, "Fuzzy model for predicting the number of deformed wheels," *Metalurgija*, vol. 55, no. 1, pp. 87–90, 2016.

[19] A. Andrade and J. Stow, "Statistical modelling of wear and damage trajectories of railway wheelsets," *Qual. Rel. Eng. Int.*, vol. 32, no. 8, pp. 2909–2923, Dec. 2016.

[20] P. Han and W.-H. Zhang, "A new binary wheel wear prediction model based on statistical method and the demonstration," *Wear*, vols. 324–325, pp. 90–99, Feb. 2015.

[21] J. J. Ding, S. L. Sun, Z. Qi, Y. H. Hiang, and F. Li, "Wheel wear prediction of railway freight car based on wheel/rail creep mechanism," *Tribology*, vol. 33, no. 3, pp. 236–244, 2013.

[22] G. Q. Tao, X. Li, Y. G. Deng, T. S. Deng, Z. F. Wen, and L. Li, "Wheel wear life prediction based on lateral motion stability of vehicle system," *Chin. J. Mech. Eng.*, vol. 49, no. 10, pp. 28–34, May 2013.

[23] R. Arno, N. Dowling, and R. J. Schuerger, "Equipment failure characteristics and RCM for optimizing maintenance cost," *IEEE Trans. Ind. Appl.*, vol. 52, no. 2, pp. 1257–1264, Mar./Apr. 2016.

[24] I. S. Apezetxea, X. Perez, C. Casanueva, and A. Alonso, "New methodology for fast prediction of wheel wear evolution," *Vehicle Syst. Dyn.*, vol. 55, no. 7, pp. 1071–1097, 2017.

[25] S. Pradhan, A. Samantaray, and R. Bhattacharyya, "Application of semi-hertzian approach to predict the dynamic behavior of railway vehicles through a wear evolution model," *J. Friction Wear*, vol. 38, no. 6, pp. 437–443, Nov. 2017.

[26] J. F. Archard, "Contact and rubbing of flat surface," *J. Appl. Phys.*, vol. 24, no. 8, pp. 918–988, 1953.

[27] T. Jendel, "Prediction of wheel profile wear—Comparisons with field measurements," *Wear*, vol. 253, nos. 1–2, pp. 89–99, Jul. 2002.

[28] S. Chen, L. Wu, H. Zhang, Z. Wen, and H. Wang, "Influence of temperature rising of tread braking on wheel wear for heavy haul freight car," *J. Mech. Eng.*, vol. 53, no. 2, pp. 92–98, Jan. 2017.

[29] P. Vila, L. Baeza, J. Martínez-Casas, and J. Carballeira, "Rail corrugation growth accounting for the flexibility and rotation of the wheel set and the non-Hertzian and non-steady-state effects at contact patch," *Vehicle Syst. Dyn.*, vol. 52, no. 1, pp. 92–108, 2014.

[30] S. Pradhan, A. K. Samantaray, and R. Bhattacharyya, "Prediction of railway wheel wear and its influence on the vehicle dynamics in a specific operating sector of Indian railways network," *Wear*, vols. 406–407, pp. 92–104, Jul. 2018.

[31] A. Saidova and A. Orlova, "Refining the parameters of Archard's wear model for calculating wear of wheels applied for 25 t per axle freight wagons on russian railways," *Vehicle Syst. Dyn.*, vol. 52, no. 1, pp. 3–15, 2014.

[32] M. A. Cremona, B. Liu, Y. Hu, S. Bruni, and R. Lewis, "Predicting railway wheel wear under uncertainty of wear coefficient, using universal kriging," *Rel. Eng. Syst. Saf.*, vol. 154, pp. 49–59, Oct. 2016.

[33] X. Yang, J. Liu, Y. Lu, L. Zhang, and Y. Gao, "Optimization of frequency conversion excitation vibration and simulation test on chaotic state in a vibration mill," *J. Vibrat. Shock*, vol. 36, no. 20, pp. 44–51, Oct. 2017.

[34] Y. Yuan, L. Qiang, G. Yang, and S. O. Mechanical, "Influence of lateral vibration on wheel polygonization," *J. Beijing Jiaotong Univ.*, vol. 40, no. 1, pp. 80–85, 2016.

[35] C. I. Barbinta and S. Cretu, "Modification of wheel-rail contact parameters by wear," *J. Balkan Tribological Assoc.*, vol. 19, no. 3, pp. 412–418, 2013.

[36] W. Xiang and G. Shen, "Simulation and improvement of the car following model concerning vehicle features," *J. East China Jiaotong Univ.*, vol. 31, no. 3, pp. 1–5, 2014.

[37] W. Shen and G. Shen, "Research on contact-detecting alarm device of wheel-set tread and flange wear," *J. East China Jiaotong Univ.*, vol. 30, no. 6, pp. 40–43, 2013.

[38] T. M. Alkhamis and M. A. Ahmed, "A modified Hooke and Jeeves algorithm with likelihood ratio performance extrapolation for simulation optimization," *Eur. J. Oper. Res.*, vol. 174, no. 3, pp. 1802–1815, Nov. 2006.

[39] K. Bamdad, M. E. Cholette, L. Guan, and J. Bell, "Ant colony algorithm for building energy optimisation problems and comparison with benchmark algorithms," *Energy Buildings*, vol. 154, pp. 404–414, Nov. 2017.

[40] M. Fries, M. Kruttschnitt, and M. Lienkamp, "Operational strategy of hybrid heavy-duty trucks by utilizing a genetic algorithm to optimize the fuel economy multiobjective criteria," *IEEE Trans. Ind. Appl.*, vol. 54, no. 4, pp. 3668–3675, Jul./Aug. 2018.

[41] J. M. N. González, J. A. Jiménez, and J. C. D. López, "Optimizing failure prediction time windows through genetic algorithms and random forests," *IEEE Access*, vol. 6, pp. 58307–58323, 2018.

[42] T. Ballal, M. A. Suliman, and T. Y. Al-Naffouri, "Bounded perturbation regularization for linear least squares estimation," *IEEE Access*, vol. 5, pp. 27551–27562, 2017.

[43] H. K. Abdulkhader, J. Jacob, and A. T. Mathew, "Fractional-order lead-lag compensator-based multi-band power system stabiliser design using a hybrid dynamic GA-PSO algorithm," *IET Gener., Transmiss. Distrib.*, vol. 12, no. 13, pp. 3248–3260, Jul. 2018.

[44] D. Goeke, "Granular Tabu Search for the pickup and delivery problem with time windows and electric vehicles," *Eur. J. Oper. Res.*, vol. 278, pp. 821–836, Nov. 2019.

[45] Z. C. Cao, Z. Z. Yuan, and D. W. Li, "Optimization of stop-skip train operation scheme for urban rail transit," *J. China Rail Way Soc.*, vol. 39, no. 11, pp. 15–22, 2017.

[46] K. A. Dowsland and J. M. Thompson, "Simulated annealing," in *Handbook of Natural Computing*, Berlin, Germany: Springer, 2012.

[47] Y. X. Li, Z. L. Xiang, and J. N. Xia, "Dynamical system models and convergence analysis for simulated annealing algorithm," *Chinses J. Comput.*, vol. 42, no. 6, pp. 1161–1172, 2019.

[48] J. Piotrowski, S. Bruni, B. Liu, and E. Di Gialleonardo, "A fast method for determination of creep forces in non-hertzian contact of wheel and rail based on a book of tables," *Multibody Syst. Dyn.*, vol. 45, no. 2, pp. 169–184, Feb. 2019.

[49] J. J. Kalker, "A fast algorithm for the simplified theory of rolling contact," *Vehicle Syst. Dyn*, vol. 11, no. 1, pp. 1–13, 1982.

[50] K. E. Zaazaa and A. L. Schwab, "Review of joost kalker's wheel-rail contact theories and their implementation in multibody codes," in *Proc. ASME Conf.*, Jan. 2009, pp. 1889–1900.

[51] J. Hejselbæk, J. Ø. Nielsen, W. Fan, and G. F. Pedersen, "Empirical study of near ground propagation in forest terrain for Internet-of-Things type device-to-device communication," *IEEE Access*, vol. 6, pp. 54052–54063, 2018.

AIHUA ZHU was born in Wuyuan, Jiangxi, China, in 1977. She received the B.S. degree in mechanical engineering from the Wuhan University of Technology, China, in 1999, and the M.S. degree in mechanical engineering from Zhejiang University, Hangzhou, China, in 2004. She is currently pursuing the Ph.D. degree in mechanical engineering with Beijing Jiaotong University, Beijing, China.

Since 2012, she has been an Assistant Professor with the School of Mechanical-electronic and vehicle Engineering, Beijing University of Civil Engineering and Architecture. She is also the Director of Super Large Construction Transportation Vehicle Branch of China Construction Machinery Association. She is the author of two books, more than 20 articles, and more than six inventions. Her research interests include vehicle system failure modeling, safety analysis, and wheel-rail relationship. She was a recipient of the outstanding teacher of Beijing University of Civil Engineering and Architecture, in 2015, and the Beijing Teaching Achievement Award First Prize, in 2018.

SI YANG was born in China, in 1994. He received the B.S. degree in mechanical engineering from the Beijing University of Civil Engineering and Architecture, in 2016, where he is currently pursuing the M.S. degree in mechanical engineering.

In 2016, he began to study the signal extraction of weak mechanical equipment faults, and used advanced noise reduction methods to analyze time-frequency signals. In 2017, he began to focus on the parameter optimization research of the mathematical model of communication systems. In 2017, the numerical simulation method was used to study the service performance and evolution of metro wheels. The current research direction is the development of complex mechanical equipment fault prediction and health management systems. He is a member of the Beijing Key Laboratory of Performance Guarantee on Urban Rail Transit.

QIANG LI was born in Shanxi, China, in 1963. He received the B.S. degree in mechanical engineering from Tianjin University, in 1984, the M.S. degree from the Huazhong University of Science and Technology, in 1989, and the Ph.D. degree in mechanical engineering from Beijing Jiaotong University, Beijing, in 1995.

Since 1998, he has been a Professor with the School of Mechanical and Electronic Control Engineering, Beijing Jiaotong University. He is the author of three books, more than 80 articles, and more than 20 inventions. His research interests include structural fatigue strength and structural reliability. Prof. Li is a member of the Reliability Committee of the Institute of Mechanical Engineering and a Senior Member of China Society of Mechanical Engineering. He was a recipient of the Top Talents in Science and Technology of the Ministry of Railways, in 1998, and the Second Prize for Scientific and Technological Progress of the Ministry of Railways, in 2007.

JIANWEI YANG was born in Henan, China, in 1971. He received the B.S. degree in mechanical engineering from the Taiyuan Heavy Machinery Institute, in 1994, the M.S. and Ph.D. degrees in mechanical engineering from the China Academy of Railway Sciences, Beijing, in 2006.

He is currently a Professor with the School of Mechanical-Electronic and Vehicle Engineering, Beijing University of Civil Engineering and Architecture. He is also the Director of the Beijing Key Laboratory of Performance Guarantee on Urban Rail Vehicles. He is the author of ten books, more than 130 articles, and more than ten inventions. His research interests include vehicle system failure modeling and safety analysis, monitoring technology and fault diagnosis, and vehicle system dynamics and control. Prof. Yang has been selected as a member for Beijing High-Creation Program, Tens of Millions of Talents Project, and Beijing Great Wall Scholars. He is a Senior Member of China Society of Mechanical Engineering and an Editorial Board of the *Journal of Internal Combustion Engine Science*.

CAOZHENG FU was born in China, in 1995. He received the B.S. degree in mechanical engineering from the Taiyuan University of Science and Technology. He is currently pursuing the M.S. degree in mechanical engineering with the Beijing University of Civil Engineering and Architecture. His research interests include wheel-rail relationship and rail transit operation and maintenance. He is also a member of the Beijing Key Laboratory of Performance Guarantee on Urban Rail Transit Vehicles.

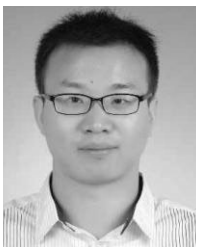

JIAO ZHANG received the B.S. and M.S. degrees in mechanical engineering from the Beijing University of Civil Engineering and Architecture, in 2012.

From 2012 to 2014, he was a Research Assistant with CRRC Beijing Nankou Company, Ltd. Since 2016, he has been a Senior Engineer with the Beijing Subway Operation Technology Centre. His research interest includes rail vehicle system failure modeling and safety analysis. He was a recipient of the Excellent Paper Award of the Third National Academic Conference on Smart Cities and Rail Transit, in 2016.

DECHEN YAO received the Ph.D. degree from the School of Traffic and Transportation, Beijing Jiaotong University, Beijing, China, in 2015. He is currently with the Beijing University of Civil Engineering and Architecture. His current research interest includes vehicle system failure diagnosis and dynamics.